Construction and Building Materials 207 (2019) 158–173

Contents lists available at ScienceDirect

Construction and Building Materials

journal homepage: www.elsevier.com/locate/conbuildmat

Mechanical and durability performance of FRP confined and unconfined strain hardening cementitious composites exposed to sulfate attack

Alaa Mohammedameen [b,c,*], Mehmet Eren Gülşan [a], Radhwan Alzeebaree [b,c], Abdulkadir Çevik [a], Anıl Niş [d]

[a] Department of Civil Engineering, Gaziantep University, Gaziantep, Turkey
[b] Department of Civil Engineering, Duhok Polytechnic University, Duhok, Iraq
[c] Department of Architecture, Nawroz University, Duhok, Iraq
[d] Department of Civil Engineering, Istanbul Gelisim University, İstanbul, Turkey

HIGHLIGHTS

- FRP confined/unconfined SHCC specimens were exposed to magnesium sulfate ($MgSO_4$).
- Investigated the effects of magnesium sulfate on the performance of SHCC specimens.
- Unconfined/confined SHCC specimen were tested under monotonic and cyclic loading.
- Type of fiber-reinforced polymer (FRP) fabric (BFRP vs CFRP) was investigated.
- Effect of type of FRP fabrics and fly ash were experimentally evaluated.
- Microstructure of SHCC exposed to magnesium sulfate was compared.
- SEM images revealed that HCFA-SHCC was more affected by sulfate than LCFA-SHCC.
- CFRP wrapped specimens were more ductile, strong and durable than BFRP wrapped ones.

ARTICLE INFO

Article history:
Received 29 May 2018
Received in revised form 7 February 2019
Accepted 17 February 2019
Available online 25 February 2019

Keywords:
Strain Hardening Cementitious Composite (SHCC)
Fiber Reinforced Polymer (FRP)
Static and Cyclic Loading
Sulfate Attacks

ABSTRACT

In this study, the performance of Fiber Reinforced Polymer (FRP) confined and unconfined Strain Hardening Cementitious Composite (SHCC) specimens exposed to sulfate attack under static and cyclic loading were investigated. Two types of FRP fabrics (Basalt (BFRP) and Carbon (CFRP)) and two types of fly ash (Low calcium (LCFA) and high calcium (HCFA)) were studied. In addition, FRP fabrics as a rehabilitation material was also investigated for the sulfate deteriorated specimens. LCFA-SHCC specimens showed superior performance than HCFA-SHCC specimens in the sulfate environment. In addition, confined specimens with FRP fabrics significantly improved compressive strength, ductility, and durability of the specimens.

Published by Elsevier Ltd.

1. Introduction

Recently, existing studies on the durability of concrete focused significantly on the chemical attacks especially in an urban region due to the significant increase in population, the number of the factory as well as hazardous waste. The deterioration of conventional concrete under chemical attacks is a recognized topic among investigators and ongoing investigates continue to prevent concrete structure deterioration under chemical attacks. In addition to chemical attacks, structures are exposed to axial loads, shear forces and bending moments, especially in earthquake zones. In such a situation, structures experience seismic loads after the loss of mechanical strength due to chemical attack and failure of the structures become inevitable.

One of the most well-known and efficient strain-hardening cementitious composite (SHCC) types is Engineered Cementitious Composite (ECC). SHCC exhibits high ductility and allows the creation of multiple micro-cracks under uniaxial tensile and flexural

Abbreviations: FRP, Fiber Reinforced Polymer; SHCC, Strain Hardening Cementitious Concrete; BFRP, Basalt Fiber Reinforced Polymer; CFRP, Carbon Fiber Reinforced Polymer; LCFA, Low Calcium Fly Ash; HCFA, High Calcium Fly Ash; LCFA-SHCC, Low Calcium Fly Ash Strain Hardening Cementitious Composite; HCFA-SHCC, High Calcium Fly Ash Strain Hardening Cementitious Composite; ECC, Engineered Cementitous Composite; PVA, Poly-vinyl Alcohol; HRWRA, High Range Water Reducing Admixture; SEM, Scanning Electron Microscopy; GLM-ANOVA, A General Linear Model Analysis of Variance.

* Corresponding author at: Department of Civil Engineering, Duhok Polytechnic University, Duhok, Iraq.
E-mail address: alaa.mohammedameen@dpu.edu.krd (A. Mohammedameen).

https://doi.org/10.1016/j.conbuildmat.2019.02.108
0950-0618/Published by Elsevier Ltd.

loadings, which makes SHCC exhibits performance under static and cyclic (earthquake) loading much more than ordinary concrete. In addition, SHCC has also higher fatigue life due to fiber bridging controlled crack propagation [1]. Governing the micro-crack propagation slows down or prevents the degradation rate due to chemical attacks and increase the structural service life [2].

Utilization of fiber reinforced polymers (FRP) in last decades as an externally wrapping have attained significant approval for repairing and strengthening the concrete structures [3]. The wrapping of reinforced concrete columns is one of the most common techniques of FRP strengthening to improve their axial strength, seismic resistance, and shear strength. In this technique, the FRP sheets are usually wrapped around the columns generally in the circumferential (hoop) direction with fibers oriented. The fiber sheet increases the axial strength by confining the concrete and producing a triaxial stress form. The FRP confinement also improves the shear resistance of concrete members and avoid early failures when concrete members are exposed to external loadings typical to the loading detected in earthquakes [4–6].

Investigation on the mechanical properties of FRP composite with concrete has been widely investigated. International design codes and specifications for the strengthening of concrete members using externally wrapped FRP jacket systems have been published [7–10]. The preference of FRP fabrics for strengthening and repairing aims can be attributed to lightweight, low thermal conductivity, and high durability performance to corrosion and chemical attacks [11–13]. The service life and durability of structures depend on the environmental factors which it is exposed. The most popular environmental attacks for concrete structures are temperature fluctuations, wind effects and wetting-drying [14]. One of the main deterioration problems took place in the cement-based materials like mortars, concrete and buildings are the sulfate attack. Sulfate ions in groundwater, soil, and seawater may deteriorate the reinforced concrete structures via causing expansion and spalling resulted by many factors like type of sulfate cation, type of cement, the concentration of sulfate and the exposure time. Many building deteriorated by sulfate usually require rehabilitation or, in most violent situations, structures require to be rebuilt [15,16]. Basalt and carbon FRP fabrics showed superior durability against environment attack [17]. The effect of salt and other chemical solutions on FRP was similar to the effects of water exposure. The main factor is the moisture that penetrates the composite which led to swelling the matrix material and relax. Moreover, concrete pore water can create alkali solutions that have high pH values between 12 and 13. The influence of these solutions on the polymer matrix is more than the influence of water. The alkali affects the polymer matrix and increases the degradation [18,19]. Investigations have indicated that the chemical solutions react with the polymer matrix and/or fibers and alters the chemical composition which affects the bond between the fibers and polymer matrix and results in a reduction in mechanical properties [20,21]. Stress corrosion is considered a common failure resulted in the chemical attack when the internal strength of the material is decreased by penetration of chemical solution under prolonged internal stress [20,21].

Although there are few investigations which study the sulfate attack on SHCC specimens, there is limited or lack of investigation related the influence of sulfate attack on SHCC specimens confined by basalt and carbon FRP fabrics under static and cyclic loading. In the scope of the study, the effect of the magnesium sulfate on the compressive strengths of the local concrete elements was investigated. For the concrete elements, the most important parameters are both compressive strength and the ductility (especially post-peak region performance). In addition, cyclic loading was also applied to some of the specimens to represent the earthquake behavior under sulfate exposure attack. Therefore, compressive strength and ductility performance of the local column elements due to magnesium sulfate attack was investigated under static and cyclic loadings in the study. The different FRPs on the strength and durability performances of local concrete elements is also investigated under static and cyclic behavior. Since there is a limited study regarding the confined concrete under cyclic loading after chemical exposure, this study aims to improve the knowledge regarding this issue. In addition, the confined concrete behavior after chemical exposure under cyclic loading can be significant in the seismic regions. Moreover, the utilization of FRP materials as a structural rehabilitation material at sulfate environment is also studied. Influences of sulfate on physical and mechanical properties involving compressive strength, visual appearance, and weight change were investigated within the investigation. Furthermore, scanning electron microscopy (SEM) analysis was achieved to clarify the influence of the sulfate attack on the inner parts of confined and unconfined SHCC specimens in micro-scale. The obtained outcomes of the investigation can be significant for local column elements exposed to sulfate attack and they can be utilized to enhance the service life of the local column elements. It should be emphasized that the outcomes of this study may not represent the behavior of whole columns or structure. However, if the behavior of local column elements under sulfate attacks can be understood thoroughly, it can give an idea about the behavior of the structure exposed to sulfate attack, and therefore, required precautions can be taken to improve the service life of the structures.

2. Experimental studies

2.1. Materials and mixture proportions

The materials used in strain hardening cementitious composite (SHCC) mixtures were; Ordinary Portland Cement (OPC), F-type fly ash (LCFA), C-type fly ash (HCFA), poly-vinyl alcohol (PVA) fibers, silica sand, water and a high range water reducing admixture (HRWRA). The chemical compositions and physical properties of the FA and OPC are presented in Table 1.

Table 2 illustrates the PVA fiber properties used in ECC concrete. To tailor the interfacial properties between fiber and matrix for SHCC performance, the PVA fibers surface is coated with a proprietary hydrophobic oiling agent of 1.2% by mass [22]. The increase in the aggregate size may have an adverse influence on ductility properties of SHCC [23], therefore silica sand with an average and maximum grain size of 110 μm and 200 μm respectively were utilized in the study. Table 3 represents the mix design of the SHCC. The fly ash to OPC ratio of 1.2 and the ratio of silica sand to the binder were 0.36 by weight. Investigation showed that water to binder ratio of 0.3 was optimum amount for both strain hardening behavior of SHCC and high rheological behavior with good fiber dispersion [24,25]. Therefore, the water to binder ratio was selected as 0.27 in this study, which was lower the specified value and expected to achieve better strain hardening behavior. To obtain the desired fresh properties, high range water reducing admixture was also added to the SHCC mixes as specified by Yang et al [26]. As a result, two mixes were produced as HCFA-SHCC mix (produced with high calcium C-type fly ash) and LCFA-SHCC mix (produced with low calcium F-type fly ash) in the study.

In this study, SHCC specimens were confined by uni-directional basalt fiber reinforced polymer (BFRP) and carbon fiber reinforced polymer (CFRP) fabrics to detect the durability and mechanical performance of these materials under sulfate attack. Table 4 shows the mean values of the mechanical and physical properties of the FRP materials, which were taken by the fabric manufacturer. Teknobond 300 Tix, free solvent, thixotropic and epoxy was utilized. It has two components; A and B are liquid resin and hardener, respectively. The mechanical properties are taken from the

Table 1
Chemical composition and physical properties of F and C type fly ashes and OPC.

Component	CaO	SiO_2	Al_2O_3	Fe_2O_3	MgO	SO_3	K_2O	Na_2O	Loss onIgnition	Specific Gravity	Blaine Fineness (m^2/kg)
Fly ash-F (%)	1.60	62.53	21.14	7.85	2.4	0.10	0.73	2.45	2.07	2.30	387
Fly ash-C (%)	15.5	46.97	11.86	7.98	6.51	3.47	3.23	2.33	0.45	2.27	306
OPC (%)	62.58	20.25	5.31	4.04	2.82	2.73	0.92	0.22	3.02	3.15	326

Table 2
The properties of PVA fibers.

Fiber Type	Tensile Strength (MPa)	Modulus of Elasticity (GPa)	Elongation (%)	Diameter (μm)	Length Density (mm) (g/cm^3)
PVA	1620	42.8	6	39	8 1.3

Table 3
Typical mix design of SHCC specimens.

Cement	Water	Microsilica sand	Fly ash	HRWRA*	Fiber (%)
1.00	0.56	0.8	1.2	0.013	2.00

* HRWRA = High range water reducing admixture; all ingredients proportion, by weight, except for fiber.

adhesive data sheets and the properties were given in Table 5. The application of the epoxy-based adhesive to the SHCC specimens was attained according to the user guide of the technical document.

2.2. Specimen preparation and curing condition

Cylinder specimens with dimensions of 100 mm and 200 mm in diameter and length respectively were cast to evaluate the compressive strength of SHCC specimens. After 24 h, specimens were demolded and cured in water at 23 ± 2 °C for 28 days. Then specimens were left in an ambient condition for drying. After required strength, three layers of carbon and basalt fiber reinforced polymer (FRP) wrappings were realized on certain specimens according to the FRP application procedure as shown in Fig. 1.

In the first step of the FRP application procedure, the surface of the specimen was prepared by removing the residual powders using a wire brush and cleaning the surface from remaining powders using an air compressor. In the second step, the sheet of FRP fabrics were prepared by cutting the sheet with a length of 115 cm (three-layer continuous wrapping length with an overlaps of 15 cm between layers) and width of 19 cm (left 0.5 cm at both top and bottom side of cylinder specimen to avoid axial load on FRP sheet). In the final step, application of FRP fabrics was attained by saturation inner sides of the FRP fabrics with epoxy resin and specimens were placed inside of the FRP fabrics, then three layers wrapping process were achieved with epoxy resin. In the FRP application process, to eliminate and fill the pores on the surface of the specimen and to get the excellent bond between concrete and FRP fabrics, the surface of the specimens was also coated with epoxy resin. In addition, the orientation of fibers inside FRP sheet was taken into consideration during the wrapping procedure to certify the orientation of fibers perpendicular to the axial direction of loading. To get the perfect bond between FRP layers and to avoid slippage of the FRP layers, an overlap length of 15 cm was provided for the outermost layers of FRP sheet. During the wrapping process, separation of fibers from the edge of FRP sheets was avoided to prevent early failure of the specimens. After FRP wrapping process, specimens were left at room temperature for 7 days to achieve the targeted strength of the epoxy resins. After the three-layer of wrapping period, the thicknesses of the FRP sheets was determined using caliper as 0.9 mm outside from the overlap region.

2.3. Specimens for mechanical tests

As a result of the fiber reinforced polymer (FRP) wrapping process, three types of specimens were obtained; control (unconfined), specimens confined by basalt FRP (BFRP) and specimens confined by carbon FRP (CFRP). Furthermore, two mixes were produced; high calcium fly ash-strain hardening cementitious composite (HCFA-SHCC) mix and low calcium fly ash-strain hardening cementitious composite (LCFA-SHCC) mix. Specimens were left under two different environments; sulfate environment and control environment (unexposed specimens). Control specimens (unexposed specimens) were tested at the ages of 28 days and 90 days, whereas specimens exposed to sulfate environment were tested at the age of 90 days; (28 days water curing and the remaining days under sulfate environment). 18 control specimens were tested at the age of 28 days (6 unconfined + 6 confined by BFRP + 6 confined by CFRP), 36 control specimens were tested at the age of 90 days (6 unconfined-static loading, 6 unconfined-cyclic loading, 6 BFRP-static loading, 6 BFRP-cyclic loading, 6 CFRP-static loading, 6 CFRP-cyclic loading). For specimens exposed to sulfate attack, 24 unconfined specimens (6 unconfined-static loading, 6 unconfined-cyclic loading, 6 unconfined-then confined (after sulfate exposure)-static loading, 6 unconfined-then confined

Table 4
The properties of fabric sheets.

FRP types	Tensile Strength (MPa)	Modulus of Elasticity (GPa)	Elongation (%)	Thickness (mm)	Area Weight (g/m^2)
BFRP	2100	105	2.6	0.3	300
CFRP	4900	240	2	0.3	300

Table 5
General properties of epoxy based adhesive material.

Epoxy Type	Pot life at 20 °C (Min)	Flexural Strength 7 days (MPa)	Compressive Strength 7 days (MPa)	Bond Strength 7 days (MPa)	Mixing ratio	Modulus of Elasticity 7 days (GPa)	Fluid density (kg/L)
Teknobond 300 Tix	30	34.16	70.81	3.45	4:1	24.61	1.02 ± 0.02

a) Concrete surface preparation

b) FRP sheets preparation

c) Application of FRP fabric

Fig. 1. Steps of applying FRP fabric.

(after sulfate exposure)-cyclic loading) and 24 confined specimens were produced (6 BFRP-static loading, 6 BFRP-cyclic loading, 6 CFRP-static loading, 6 CFRP-cyclic loading) and as a total of 48 specimens under sulfate attack were tested at the age of 90 days. It should be noticed that 12 unconfined specimens exposed to sulfate attack were later confined with FRP fabrics to examine the performances of FRP as retrofit/rehabilitation materials. Since, wrapped specimens required at least seven days to obtain the

Fig. 2. SHCC specimen under axial load.

target strength of the epoxy resin [27]. Therefore, all soaked specimens (confined and unconfined) led to dry for 24 h (confined specimens wrapped by FRP and unconfined specimens store in lab) and tested under compression after 7 days later 24 h of drying. Meanwhile, the age of compressive strength test were ((28 + 8 days) and (90 + 8 days)).

2.4. Specimens under sulfate attack

There is no typical test method presented to measure the durability of concretes under chemical attack. However, ASTM C 267 test method [28] proposes that specimens should be immersed in water for 24 h prior exposed to chemical attacks to achieve water saturated specimsens. Thus, specimens were soaked in water for 24 h and left to the drying at 23 ± 2 °C for 2 h prior to record initial saturated weights of the specimens. Then specimens were soaked in 5% sulfate solution for a period of 8-weeks. At the same period, control specimens for each different mix were stored in an ambient environment at 23 ± 2 °C in the laboratory for 8-weeks for comparison. SHCC specimens were taken from the sulfate solution after the end of each week, resulting chemical reaction on the surface of concrete were eliminated by water. The specimens were left at laboratory environment at 23 ± 2 °C for 2 h to drying prior to record the weight of the specimens.

2.5. Testing procedure

Compressive strength tests were carried out on confined and unconfined cylinder specimens under static and cyclic loadings. Compressive strength tests were carried out according to ASTM C39 [29]. All compressive strength tests were performed under displacement controlled loading with a rate of 0.2 mm/min. Two linear variable displacement transducers (LVDT) were attached to measure axial deformations in the specimens as shown in Fig. 2. Stress and strain data were obtained for each specimen.

3. Experimental results and discussion

3.1. Visual examination

Visual examination of specimens indicated after 8-weeks of sulfate exposure that there is no change in visual appearance, cracking or spalling observed on the specimens. However, a very thin layer of efflorescence was observed on the outer surface of the exposed specimens. When specimens were inspected in details, both confined and unconfined SHCC specimens and PVA fibers were deteriorated from the sulfate solution. However, the deterioration was only observed at the unwrapped part of the cylinder specimens (top and bottom parts). Due to the confinement with FRP layers in the lateral direction, no deterioration was observed as is seen in Fig. 3.

Wallah and Rangan [30] investigated the influence of 2% sulphuric acid attack on cylinder specimens with 100 mm diameter and stated that acid can penetrate only 20 mm, and the remaining 80 mm remained unaffected. In the study, the penetration depth due to sulfate attack was investigated by cutting a 1 cm slice from 100 mm cylinder specimens and the average depth of the sulfate penetration was measured as 8 mm. It was also observed that the remaining inner parts were found unaffected as shown in Fig. 3. It was clearly noticed that the sulfate damage in unconfined specimens was found more severe than the specimens confined by carbon and basalt FRP fabrics. This result was also supported by the previous study, which found out that the chemical solution is a surface phenomenon and the damage starts at the surface and progresses to the inner parts of the concrete [31]. In addition, SEM inspections were also realized from concrete slices as shown in Fig. 3.

3.2. Weight change

Fig. 4 indicates weight gain (%) of the specimens under two months of chemical exposure. Results presented that all specimens had weight gain under sulfate solution absorption, and unconfined specimens showed the highest weight gain. The gained weights were 0.98% for LCFA specimens and 1.22% for high calcium fly ash HCFA specimens. Confined HCFA also showed slightly higher weight gain than the confined LCFA specimens. Moreover, the lower weight gain showed in LCFA specimens confined by carbon FRP (CFRP) and therefore, the specimens confined by CFRP fabrics showed slightly better chemical resistance than BFRP fabrics under sulfate attack. Lower weight gains showed in confined and unconfined LCFA specimens may be due to the higher fineness ratio, which caused a reduction in porosity and reduced chemical solution absorption. The earlier research was also reported the weight gain due to chemical exposure [32,33]. The penetration of harmful actions from chemical solution reacted with cement and caused the formation of gypsum and ettringite. As a result, increased volume by a factor of about two and reduced density of concrete [34]. Therefore, initial weight gains of the specimens exposed to the chemical solution may be due to the increase in relative volume was more than the reduction amount in relative density [31].

3.3. Compressive strengths of the specimens

In general, the behaviors of SHCC specimens confined by FRP fabrics under axial load were found to be consistent with the performance of conventional concrete confined by FRP in the literature. During the early stages of the axial loading process, the noise related to the microcracking of SHCC material was clear, which indicate the beginning of the stress transfer from the expanded SHCC specimen to the FRP fabrics. The cracking noises intensity could be heard pre-failure that achieved after the slow rupture of FRP fabrics with a violent and sudden noise. Failure initiated from an overlap place of the FRP fabrics at the middle height of the specimen and moved to the bottom and top of the specimens. For the tested specimens, all failures happened as a result of the rupture of FRP fabrics followed by a ductile performance of SHCC and failure due to de-bonding was not observed in

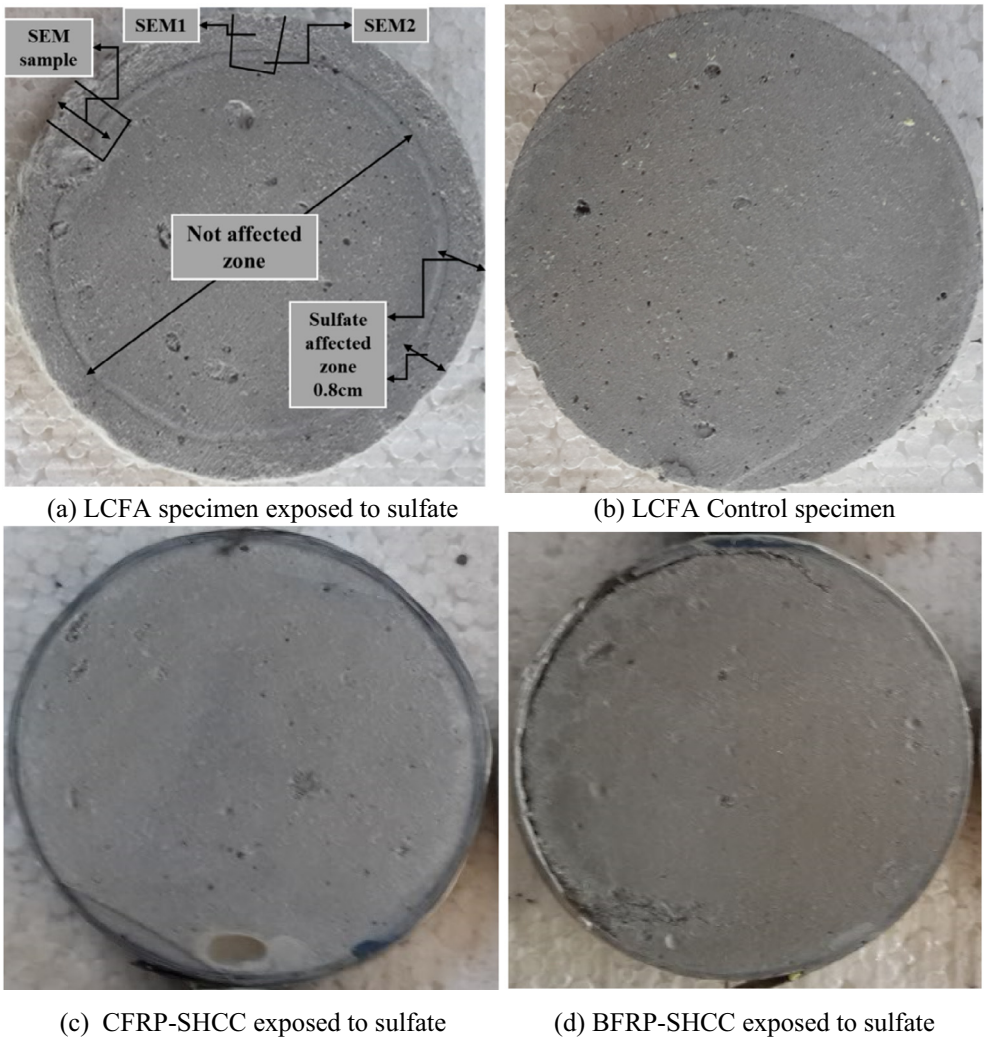

Fig. 3. Detail of SHCC showing sulfate affected zone and SEM samples places.

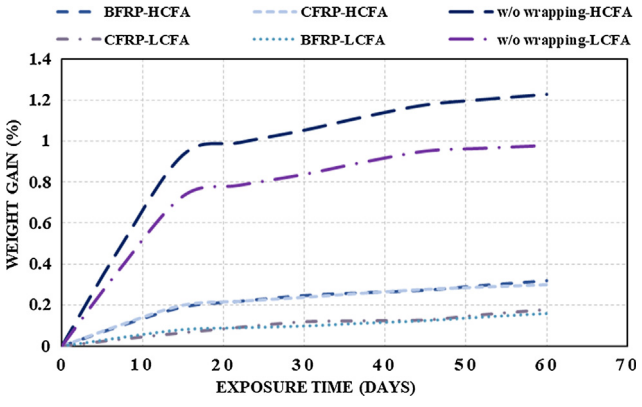

Fig. 4. Weight gain in SHCC specimens exposed to sulfate attack.

confined specimens. Table 6 represents the both average compressive strengths (AVG) and standard deviations (SD) of the specimens. Results showed that specimen confined by FRP indicated superior performance than unconfined specimens under both sulfate and ambient environments. In addition, the compressive strength of fiber reinforced cement-based composites mainly depends on the properties of the matrix. Due to the high CaO content (to form C—S—H gel) in the HCFA-SHCC specimens, the compressive strength was found more than the LCFA-SHCC specimens.

3.3.1. Compressive performance of unconfined specimens

Fig. 5 indicates typical compressive stress–strain curves of unconfined SHCC specimens. Results showed that compressive strength of unconfined specimens increased up to 90 days. The continuity of hydration reactions and the slow pozzolanic reaction of fly ash may be the reason for the increase in the compressive strength. Similar outcomes were also stated in the previous investigations [2,35].

The compressive strength values of 90-day curing specimens were 27.72% and 19.94% higher than the compressive strength values of 28-day curing for LCFA and HCFA specimens, respectively. Higher improve in the compressive strengths of LCFA specimens at 90-days ages compared to HCFA specimens was expected because of lower CaO amount in the low lime-fly ash (LCFA) specimens since the rate of hydration reactions was slow, where strength improvement (C_3S and C_2S creation) became time dependent. Reductions in compressive strength for the specimens exposed to sulfate attack were 0.17% and 14.92% for 28 days, 10% and 16.48% for 90 days strengths of LCFA and HCFA specimens, respectively. Higher reduction in compressive strength for HCFA specimens may be also attributed to high CaO content in the in the high lime-fly ash (HCFA) specimens.

Table 6
Compressive strength of LCFA and HCFA specimens.

Compressive Strength of LCFA – SHCC specimens (MPa)											
#	Control 28 days			Control 90 days			Exposed to Sulfate Attack				
	w/o wrap	CFRP	BFRP	w/o wrap	CFRP	BFRP	w/o wrap	CFRP	BFRP	CFRP-A*	BFRP-A*
AVG	21.25	60.41	42.8	27.2	75.01	53.18	24.42	73.0	51.09	71.7	50.01
SD	0.89	0.73	0.79	0.78	0.61	0.77	0.72	0.51	0.57	0.89	0.96
Compressive Strength of HCFA – SHCC specimens (MPa)											
#	Control 28 days			Control 90 days			Exposed to Sulfate Attack				
	w/o wrap	CFRP	BFRP	w/o wrap	CFRP	BFRP	w/o wrap	CFRP	BFRP	CFRP-A*	BFRP-A*
AVG	47.4	72.81	56.25	56.9	90.62	67.46	47.48	87.16	63.78	82.33	60.56
SD	0.75	0.68	0.63	0.74	0.91	0.76	0.71	0.60	0.61	0.80	0.87

* CFRP-A and BFRP-A = The specimens wrapped after exposed to sulfate by CFRP and BFRP respectively.

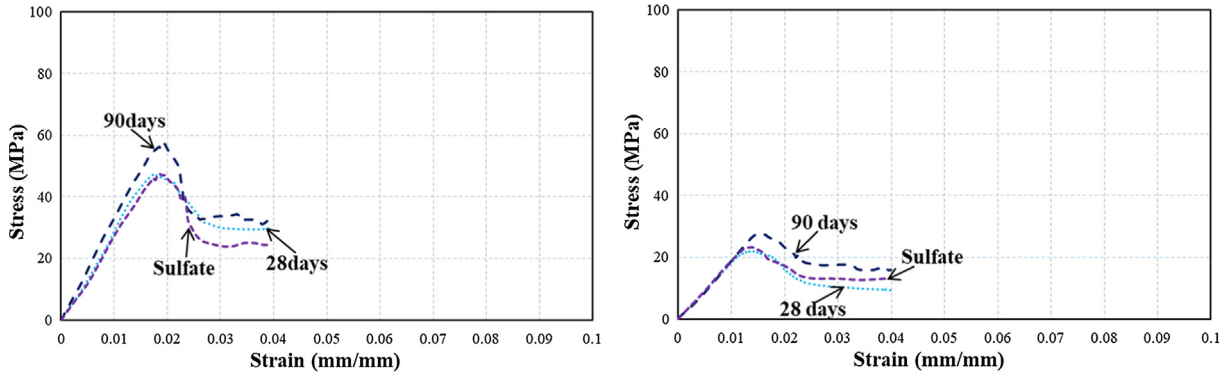

a) Unconfined HCFA-SHCC specimens b) Unconfined LCFA-SHCC specimens

Fig. 5. Stress–strain curves of unconfined SHCC specimens.

3.3.2. Compressive performance of confined specimens

Fig. 6 represents the compressive performance of confined SHCC specimens. Results showed a significant increase in compressive strength for SHCC confined by FRP fabrics (more than 2–3 times) when compared to unconfined specimens. In general, the compressive load decreased suddenly as the outermost layer of FRP fabrics ruptured and then the load started to increase or continue at a constant value due to stress move from FRP fabrics to SHCC concrete until the failure of the inner layer of FRP fibers and PVA fibers inside the SHCC specimens [36].

Similar to unconfined specimens, compressive strengths values of the confined specimens also increased up to the age of 90-days. The improvement amounts were 24.17% and 24.25% for LCFA specimens and 24.46% and 20.46% for HCFA specimens confined with CFRP and BFRP fabrics, respectively. Results showed that the influence of concrete matrix on strength values was also important when specimens confined by FRP fibers.

Compressive strengths values of the confined specimens exposed to sulfate attack at the age of 90-days were found to be greater than the compressive strengths of the confined specimens at age of 28-day. The increasing amounts were 19.71% and 13.4% for the HCFA-SHCC specimens and 20.84% and 19.37% for the LCFA-SHCC specimens confined with CFRP and BFRP fabrics, respectively. Lower increase in compressive strength for the HCFA specimens may be due to the deterioration result of CaO amount especially for the specimens includes high lime fly ash. Furthermore, the compressive strengths of the confined specimens exposed to sulfate solution at the age of 90-days were found lower than the strength of unexposed confined specimens at the age of 90-days, as predictable. The reduction amounts as a result of sulfate solution were 2.68% and 3.93% for LCFA specimens and 3.82% and 5.45% for HCFA specimens confined with CFRP and BFRP fabrics, respectively.

In this study, unconfined specimens were exposed to sulfate solution and then FRP fabrics were placed on the same specimens in order to investigate the influence of FRP fabrics as retrofit/rehabilitation materials. Results indicated that the strength of the specimens wrapped after exposed to sulfate attack (designed as Sulfate-A on Figures and BFRP-A* and CFRP-A* on Table 5) were lower than the strength of before wrapped specimens exposed to sulfate attack, as predictable. The reduction amounts were only 9.15% and 10.63% for HCFA specimens and 4.41% and 5.96% for LCFA specimens confined with CFRP and BFRP, respectively. Outcomes showed that both FRP fabrics can be also a resolution of sulfate deteriorated concrete and can be utilized as a rehabilitation or retrofit material under sulfate attack.

In addition to compressive strength, confined the specimens by FRP fabrics also increased the ductility behavior of specimens. The ductility improvement was stated in the literature for conventional concrete confined by FRP materials [4,37]. In general, SHCC specimens exhibit strain hardening behavior, which resulted in an enhanced toughness and ductility. In addition, confined SHCC specimens by FRP fabrics resulted in very high lateral displacement amounts and toughness, specially post-peak curve of the axial stress–strain curve. This outcome makes the composite FRP-SHCC important in structural fundamentals demands high strength and high ductility. In the study, carbon FRP fabrics enhanced the strain from 0.04 to 0.09 and basalt FRP fabrics improved up to 0.07 as indicated in Figs. 6 and 7 due to the effect of FRP fabric confinement, which forms a triaxial condition of the stress along the SHCC specimen height which leads to higher strength and strain amounts. After the rupture failure of FRP fabrics, SHCC concrete

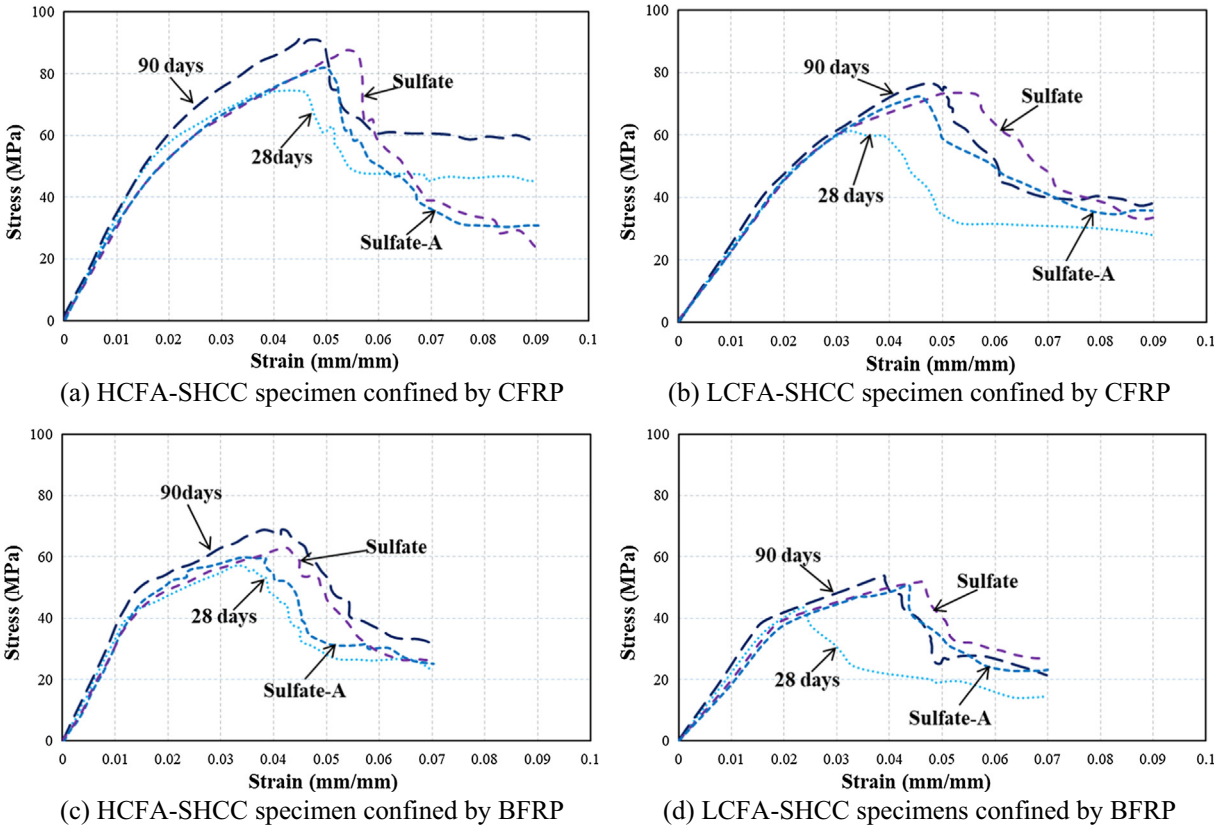

Fig. 6. Stress–strain curves of confined SHCC specimen.

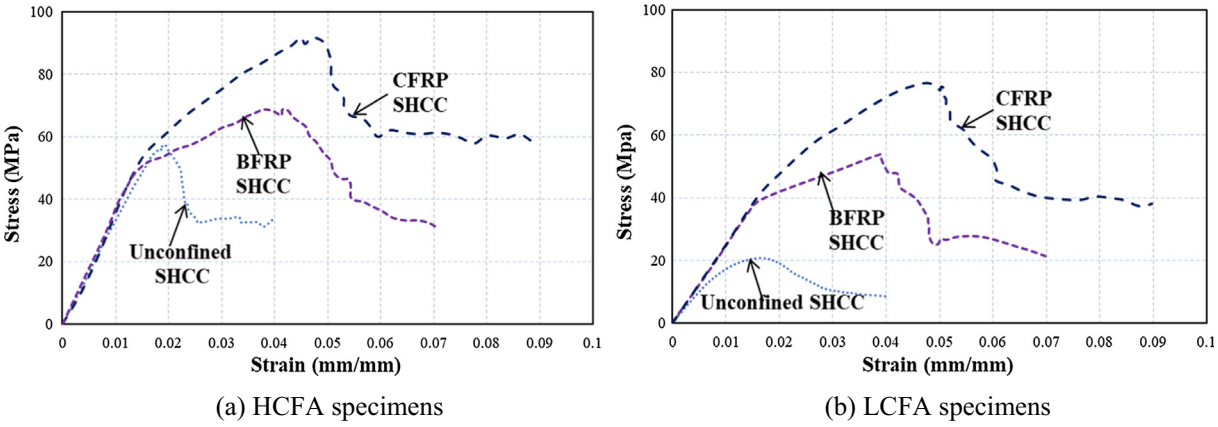

Fig. 7. Stress-Strain Curves of confined and unconfined SHCC specimen.

including PVA fibers continued to resist the axial load until failure of PVA fibers. Carbon FRP fabrics confined specimens exhibits superior strength and ductility amount than the basalt FRP fabrics confined specimens and the poor behavior was achieved in the unconfined specimens as indicated in Fig. 7.

3.3.3. Failure modes of specimens exposed to an axial compression load

During axial compression load process, the concrete expansion expected on SHCC specimens and the FRP prevented the expansion and formed a confinement in the circumferential direction along the cylinder specimens height. As tensile stresses resulted by axial load exceed the tensile strength resistance of FRP reinforced SHCC materials, first the FRP rupture happened and the resistance of axial load continued by matrix until the failure of the PVA fibers. In this study, all failure mechanism obtained due to FRP rupture followed by failure of the matrix. In the scope of the research, no de-bonding was observed during the mechanical tests; however, the de-bonding failure had rarely been stated by previous studies [38,39].

For the ordinary concretes confined by FRP fabrics, the failure mode can be characterized by crushing of concrete followed by the rupture of the FRP fabrics at the mid-height region of the cylinder specimens. In addition, vertical cracks along the specimen height are observed for the unwrapped specimens. For the wrapped specimens, more expansion is localized at the middle portions of the specimens due to the higher tensile stresses, which enables stress transfer from expanded concrete to the FRP fabrics.

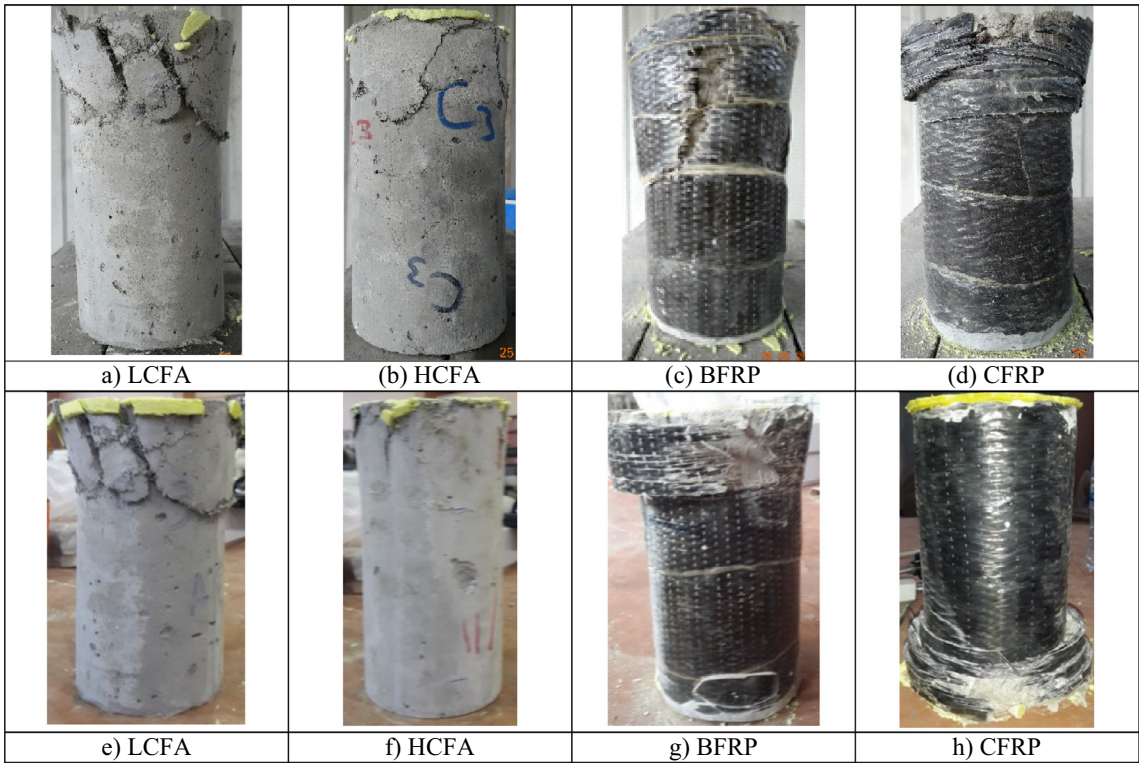

Fig. 8. Failure mode of SHCC specimens exposed to sulfate (a, b, c, d) and control (e, f, g, and h).

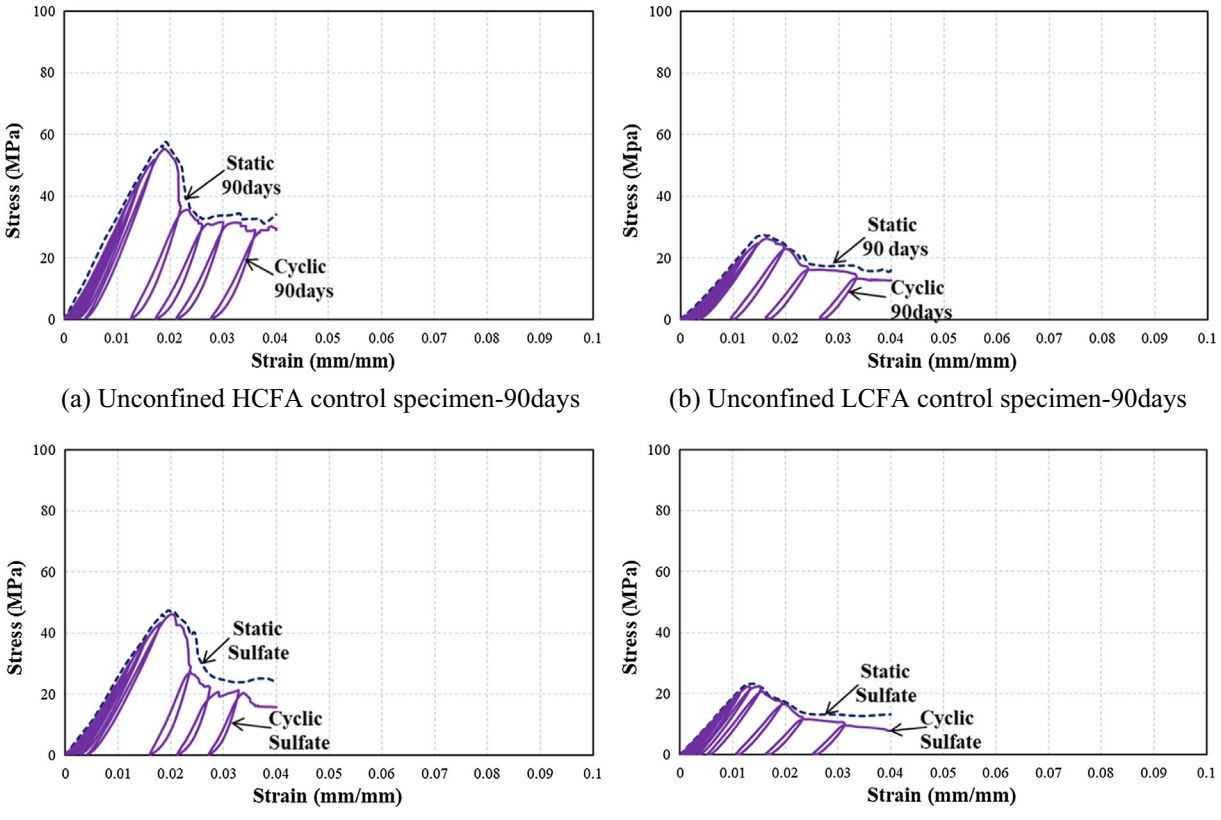

Fig. 9. Static and cyclic loading diagram of unconfined SHCC specimens.

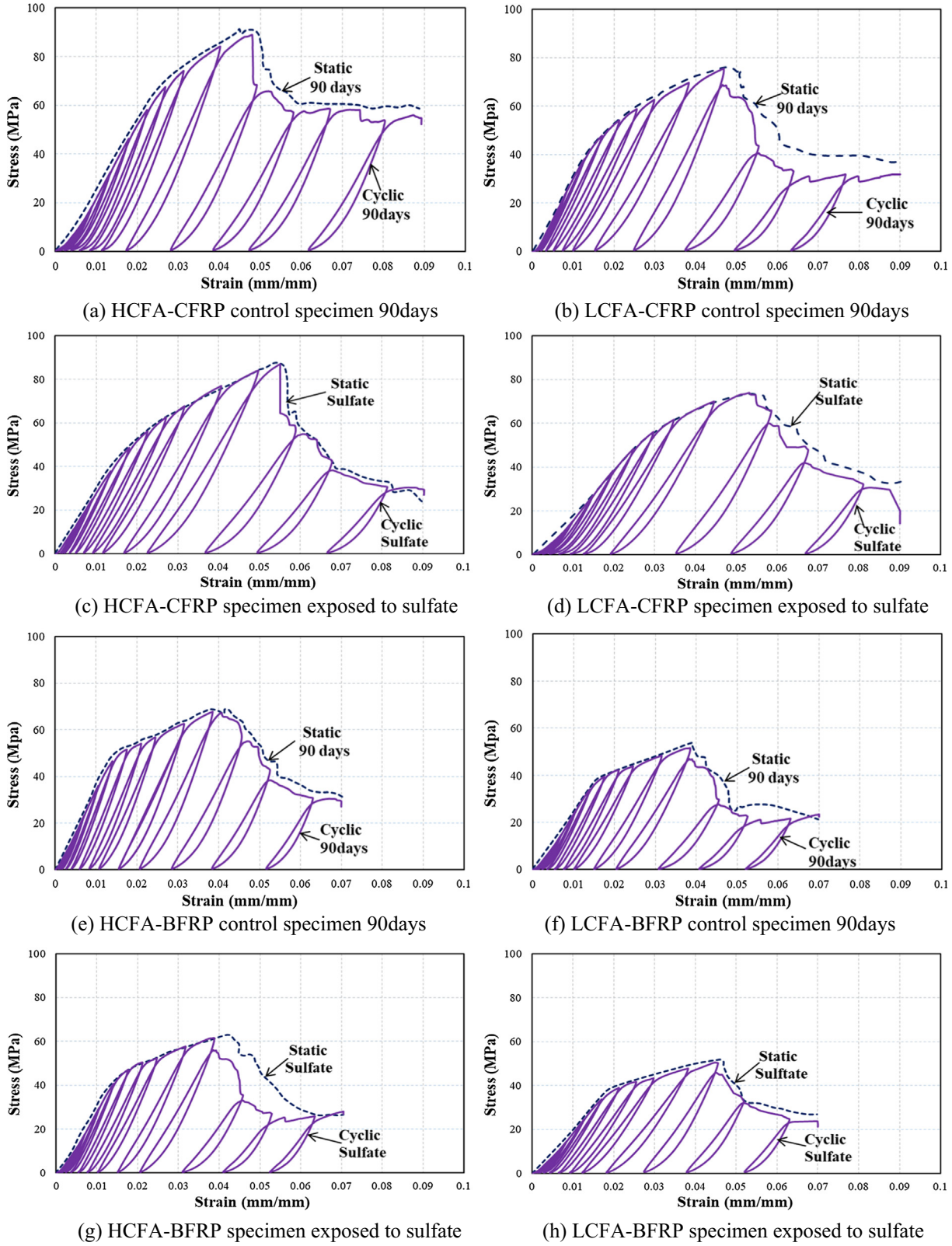

Fig. 10. Static and cyclic loading diagram for confined SHCC specimens.

For the further lateral expansion, FRP fabrics are fully activated and finally the rupture of the FRP fabric starts at the mid-height and progresses at top and bottom regions [40,41].

However, for the SHCC specimen, the failure mechanism found to be different than the ordinary concrete. The PVA-ECC concrete exhibits strain hardening behavior due to the lateral strain capability of PVA fibers, and the ductility of the SHCC specimens improves further with the utilization of the carbon and basalt FRP fabrics. Fig. 8 summarizes the fracture or failure modes of the unconfined and confined SHCC specimens. For these specimens, cracks

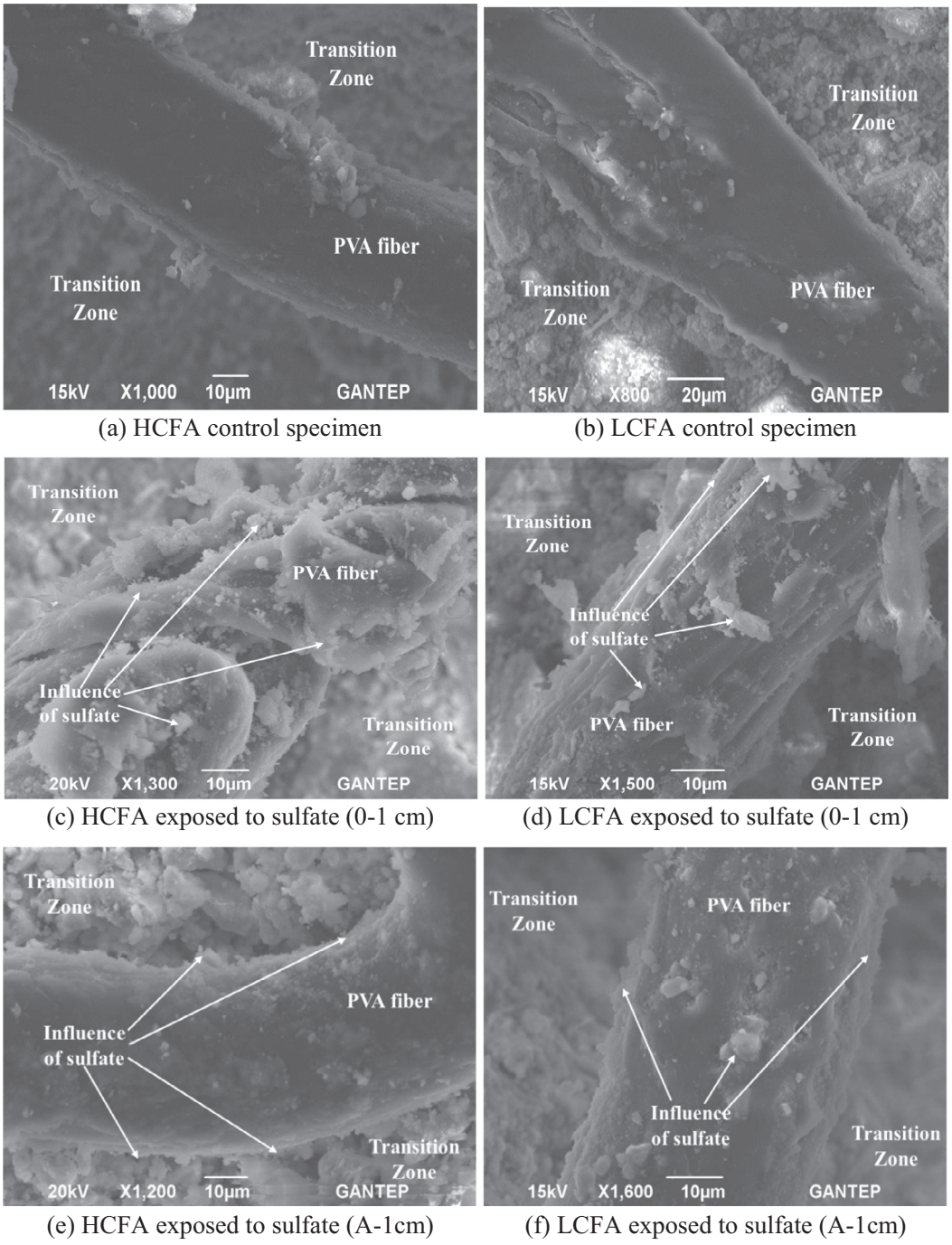

Fig. 11. SEM photos of unconfined HCFA-SHCC (left) and LCFA-SHCC (right) specimens.

initiated at the top or bottom parts of the cylinder specimen and crack openings developed until the failure occurs at these places as a result of high-stress concentrations created due to the friction between the specimen and the machine plates. As FRP fabrics were placed uni-directional, sudden failure was realized of the FRP fabrics caused by shearing off FRP fabrics and later the load transfer between FRP fibers cannot be possible. As reported in previous studies on FRP confinement concrete, low popping noises were heard during various stages of the loading process [40,41]. As the FRP fabric was taken off regarding the failure modes, it was noted obviously that the failure occurred at the bottom or top part of the specimens. The failure of the some of the ductile specimens at the top and bottom regions is also reported in the in the previous study [42].

The failure of SHCC (ductile) specimens are localized at the end portions of the specimens, while the failure of the ordinary concrete (brittle) specimens are localized at the middle portions, which indicates that friction between machine plates and specimens becomes significant for the ductile specimens. For that reason, the anti-friction devices can be used in order to eliminate the top and bottom end of the failure of the cylinder specimen as reported in the earlier studies [43,44].

In Fig. 8a and e, the failure modes of LCFA specimens were found almost the same under sulfate and control environments, which indicated that LCFA specimens does not much affect the failure mode. Concerning the HCFA specimens, the effect of sulfate solution led to a relatively negative effect (more deterioration) on the failure as can be seen in Fig. 8b and f. This could be

explained by the existence of high calcium content in HCFA specimens. When confining the specimens with basalt FRP fabrics, more deterioration was observed under sulfate solution than control environment as can be seen in Fig. 8c and g. This can be explained by the fact that basalt FRP fabric can react with the sulfate solution, leading to a weak performace agains sulfate solution. On the other hand, carbon FRP fabrics showed the same failure mode under sulfate and control environments as can be seen in Fig. 8d and h. Due to the high tensile strength capacity, failure was observed at top regions of the specimens, which can be attributed to the friction between machine plates and specimens.

Failure of the unconfined SHCC specimens occurred more violent than the specimens wrapped with FRP fabrics. Due to the high bond strength of PVA fibers, the formed cracks cannot propagate into the mid-lengths of the specimens in general [36]. The failure of the unwrapped specimens occurred near the top and bottom of the specimens as similar to the wrapped ones. However, failure of the specimens subjected to sulfate was more violent than unexposed specimens as shown in Fig. 8. This may result from gypsum and ettringite formation at the outer surface (~1 cm) under magnesium sulfate environment. The sulfate produced additional tensile stresses and caused weaknesses in the concretes. When the sulfate influence combined with the external axial load, the cracking may form at the weakest defects and further elongate along the specimen heights.

3.4. Cyclic loading behaviour

Figs. 9 and 10 illustrate the axial stress–strain curves resulted from both static and cyclic loadings of the tested specimens. Results showed that the pre-peak performance of unconfined specimens resulted from static and cyclic loading was obtained almost linear up to the peak loads even for the specimens exposed to sulfate attack as shown in Fig. 9. However, regarding the post-peak performance of unconfined specimens exposed to sulfate solution, the static and cyclic curve moved away from each other, which may be due to the extra reduction in elastic modulus resulted from softening and decreased the rigidity of specimens with an increase in loading/unloading cycles. This behavior can be detected clearly for HCFA specimens due to the high amount of CaO.

For confined specimens, the pre-peak performance of confined specimens expected as linear up to the points that match to the failure of unconfined specimens as presented in Fig. 10. After that due to the cracks formed in the SHCC matrix at higher stresses, the elastic modulus of SHCC material was decreased. However, higher stresses were achieved due to the presence of FRP fabrics. However, similar stress relaxation was also indicated in the post-peak part for both static and cyclic loadings, which may be due to the elastic performance of the FRP, which enhanced the resistance of the specimens to cyclic loadings. The favorable effect of carbon and basalt FRP material on the post-peak curve can be easily observed under sulfate attack.

The envelopes of all stress–strain curves of SHCC tested specimens under cyclic loading can be drowned by joining the peak points of the unloading cycles on the stress–strain curves and the resulted curve matches well with the resultant stress–strain curve of the specimens from static loading. Similar indications were also stated by previous studies Lam et al [45] and Shah et al [46] reported that this behavior also suitable for concretes confined by FRP fabrics. In this study, the static and cyclic loading curves of tested specimens confined by carbon FRP and basalt FRP obeyed with each other as presented in Fig. 10.

3.5. Scanning electron microscopy (SEM)

Confined and unconfined SHCC specimens were analyzed by scanning electron microscopy (SEM) in details to detect the alters in the surface of PVA fibers and the transition zone between the

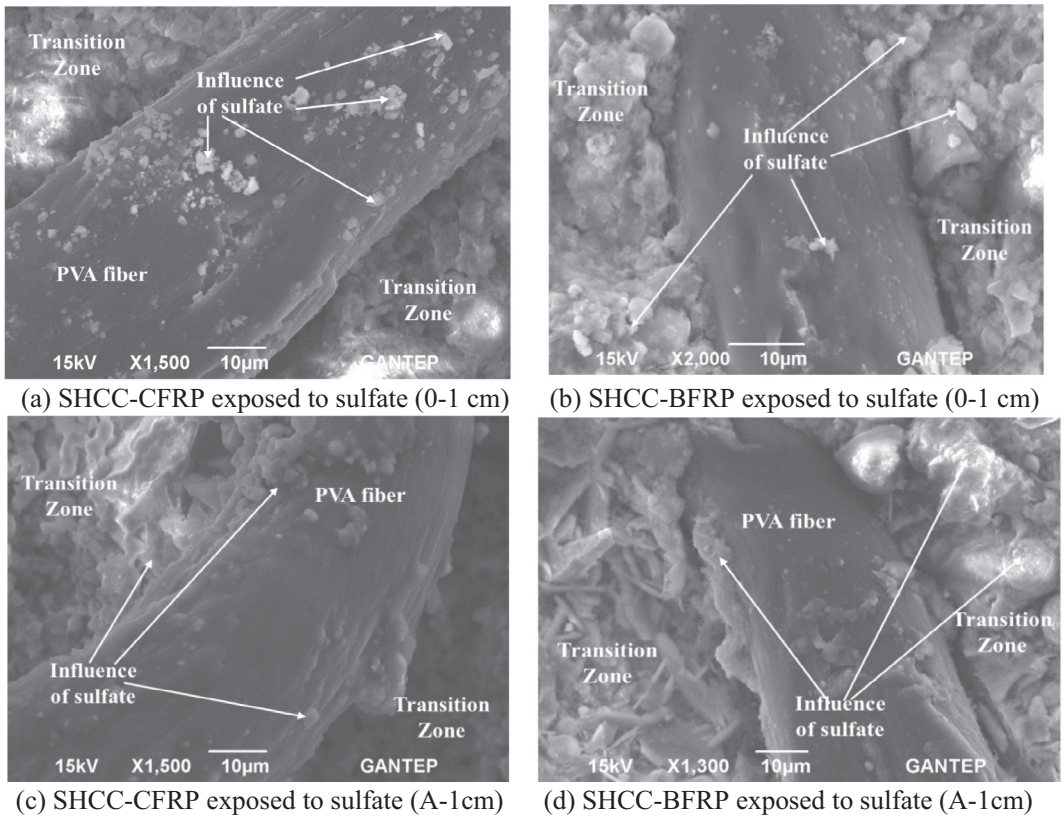

Fig. 12. SEM photos of CFRP and BFRP confined HCFA specimens.

fiber and the matrix as a result of chemical reaction of sulfate solution. In addition, the effects on the surfaces of carbon and basalt FRP fabrics were studied in microscale. In order to prepare SEM samples, one inch (2.54 cm) slices from both top and bottom sections of the specimens were cut and discarded, from the middle region of the specimens 1 cm thick circular slice was utilized for SEM analysis. The sulfate affected zone width was about 8 mm from the outer circumference of the cylinder specimen as indicated in Fig. 3. Therefore, for each specimen two SEM images were taken, one of them was taken at the sulfate influenced region (0–1 cm from the surface) and the other one was taken from the uninfluenced region (close to the influenced region but out of the 1 cm outer layer).

SEM photos of the unconfined SHCC specimens under various environments were organized in Fig. 11. SEM images of sulfate influenced region shown that white sediments created on the surface of the PVA fibers and the number of white sediments for HCFA specimens was much higher than LCFA specimens. Due to the high amount of calcium, the higher ratio of Ca/Si and the free calcium lead to high deterioration of the cement paste and creation of gypsum and ettringite which can produce expansion, dimensional instability, cracking, spalling and reduction in mechanical properties [47,48]. As specified previously, SEM photos were also taken out of the sulfate influenced region (specified as A-1) and low vitreous segments were concentrated on the surface of the PVA fibers. SEM photos specified that sulfate attacks begun from the outer layer and grew to the inside of the specimens. It was also investigated that the adverse influence of sulfate on HCFA specimens was higher than the LCFA specimens in both sulfates influenced and uninfluenced region. The white sediments also detected in the

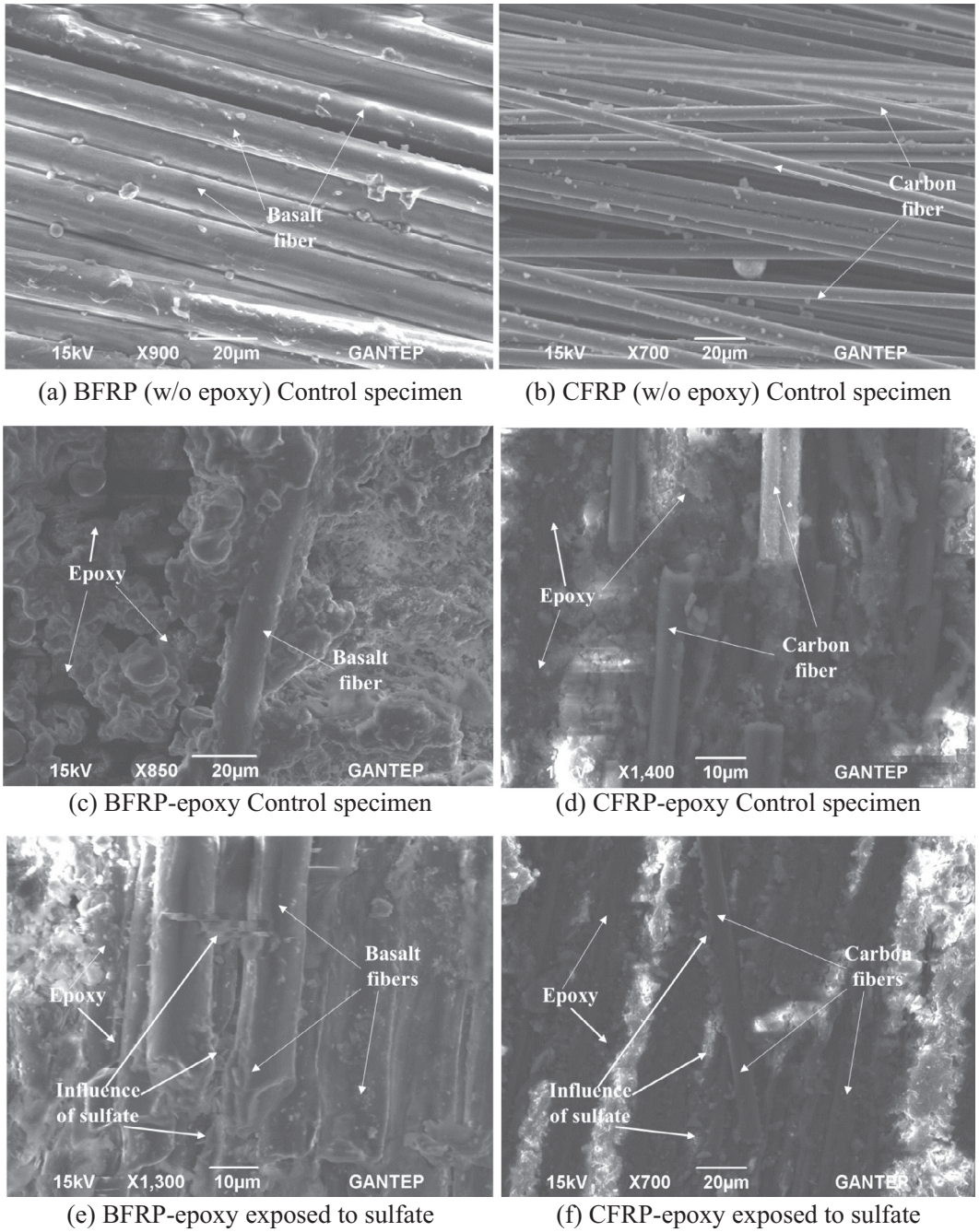

Fig. 13. SEM photos of BFRP and CFRP fabric sheets.

Table 7
Statistical evaluation of the test result.

Dependent Variable	Independent variable	Sequential Sum of Squares	Mean Square	Computed F	P Value	Significant	Contribution (%)
LCFA-SHCC	Age level	167.93	167.93	23.78	0.01	Yes	5.12
	FRP confinement	3071.47	1535.74	217.48	0.00	Yes	93.79
	Error	35.31	7.06				1.09
	Total	3274.72					
LCFA-SHCC	Sulfate Attack	7.89	7.89	88.03	0.01	Yes	0.34
	FRP confinement	2329.37	1164.69	12996.32	0.00	Yes	99.65
	Error	0.18	0.09				1.00
	Total	2337.44					
LCFA-SHCC	Age level	153.71	153.71	20.33	0.01	Yes	4.80
	FRP confinement*	3011.83	1505.92	199.18	0.00	Yes	94.02
	Error	37.80	7.56				1.18
	Total	3203.34					
LCFA-SHCC	Sulfate Attack	14.29	14.29	378.91	0.00	Yes	0.63
	FRP confinement*	2265.93	1132.96	30038.81	0.00	Yes	99.37
	Error	0.08	0.04				0.00
	Total	2280.29					
HCFA-SHCC	Age level	203.21	203.21	10.15	0.02	Yes	10.30
	FRP confinement	1668.91	834.46	41.67	0.00	Yes	84.62
	Error	100.12	20.02				5.08
	Total	1972.24					
HCFA-SHCC	Sulfate Attack	45.71	45.71	8.00	0.02	Yes	3.18
	FRP confinement	1379.17	689.58	120.77	0.01	Yes	96.02
	Error	11.42	5.71				0.79
	Total	1436.29					
HCFA-SHCC	Age level	247.30	247.30	25.68	0.04	Yes	21.05
	FRP confinement*	908.46	454.23	47.18	0.02	Yes	77.31
	Error	19.26	9.63				1.63
	Total	1175.02					
HCFA-SHCC	Sulfate Attack	100.94	100.94	126.71	0.01	Yes	7.67
	FRP confinement*	1213.23	606.62	761.49	0.00	Yes	92.21
	Error	1.59	0.80				0.12
	Total	1315.77					

FRP confinement*; SHCC specimens wrapped by FRP fabrics after exposed to sulfate attack (represents CFRP* and BFRP* in the Table 6).

interfacial transition zone, which weakened the bond between the cement matrix and PVA fibers.

SEM photos of basalt and carbon FRP confined HCFA specimens were presented in Fig. 12. Outcomes specified that PVA fibers of SHCC specimens confined by basalt and carbon FRP were deteriorated by sulfate attack less than PVA fibers of unconfined specimens. In addition, basalt and carbon FRP fibers also influenced by the sulfate attack. Due to the sensitivity of the epoxy resin to an alkaline environment, BFRP and CFRP fabrics were also substantially influenced by the sulfate solution. However, due to the higher bond between CFRP fabrics and the epoxy resin, specimens confined by CFRP fabrics were less deteriorated compared to specimens confined by BFRP fabrics as indicated in Fig. 13.

3.6. Statistical evaluation of the test result

A general linear model analysis of variance (GLM-ANOVA) was performed at a significant level of 0.05 to estimate the variation in the performance of the fiber reinforced polymer confined and unconfined strain hardening cementitous composite exposed to sulfate attack in a quantitative form. For this, the type of fly ash (LCFA-SHCC and HCFA-SHCC) were assigned as the dependent variables while age level, FRP confinement, sulfate attack, and sulfate deteriorated specimens confined by FRP fabrics (titled as FRP confinement*) were the independent factors. A statistical analysis was conducted to evaluate the statistically significant factors (p-level < 0.05). A p-value less than 0.05 showed that the related parameter is a significant factor in the test results. In addition, percent contribution was also calculated to have an idea about the degree of effectiveness of the parameter on the resulting performance. If this value is higher, then it can be accepted as the effect of the parameter is high on the resulting performance. Table 7 presents the contributions (%) of the factors on the resulting performances. The FRP confinement was found to be the most dominant factor than the effect of sulfate attack and age level for both types of fly ash. In addition, the effect of sulfate attack was also found higher than the effect of age level on the compressive strength of the specimens. Moreover, the specimens produced with low calcium fly ash (LCFA-SHCC) was found to had superior performance than the specimens produced with high calcium fly ash (HCFA-SHCC). On the other hand, specimens wrapped after exposed to sulfate (FRP confinement*) was also affected and it can be concluded that both FRP fabrics can be used as rehabilitation materials in sulfate environments.

4. Conclusion

This study investigates the degradation influence of the magnesium sulfate attack on SHCC specimens under static and cyclic loading. The specimens were also reinforced with basalt and carbon FRP fabrics to assess performances of the concretes under sulfate attack. In addition, the use of FRP material as a rehabilitation material was also evaluated. Scanning electron microscopy (SEM) analysis was also achieved to detect the changes in the surface of PVA fibers and in the interfacial transition zone between the fibers and the matrix. General findings were summarized as follows:

- Visual appearance results showed that the surface color of the specimens containing high lime fly ash (HCFA) and the specimens containing low lime-fly ash (LCFA) remained grey even after 8-weeks of exposure.
- SHCC specimens indicated superior mechanical performance and durability resistance against sulfate attacks. However, LCFA-SHCC specimens (including low lime) indicated better

performance than HCFA-SHCC specimens (containing high lime). This may be due to the high amount of CaO in HCFA specimens, which increased the creation of gypsum and ettringite and caused a reduction in mechanical behavior and durability performance.

- The utilization of FRP fabrics with the SHCC specimens enhanced substantially both compressive strength and ductility performance of specimens. Results indicated that specimens confined by carbon FRP exhibit better mechanical and durability behavior than the specimens confined by basalt FRP under both sulfate and ambient environments. The poor performance was detected in unconfined specimens
- Strengthening the SHCC specimens after exposed to sulfate attack (sulfate deteriorated specimens) in the study, improved significantly the mechanical performance and it was established that both FRP fabrics (CFRP and BFRP) can be a solution for sulfate deteriorated concrete and can be utilized as a rehabilitation or retrofit material under sulfate environment.
- The envelopes of all stress–strain curves of SHCC tested specimens achieved from cyclic loading test exhibited similar performance with the curves obtained from static loading test under ambient environment. Regarding the post-peak performance of unconfined specimens exposed to sulfate attack, the static and cyclic curve moved away from each other, especially for HCFA specimens; which may be due to the further reduction in elastic modulus under sulfate solution resulted from softening and decreased the rigidity of the concrete with an increase in loading/unloading cycles. For confined specimens cured at both ambient and sulfate environment, FRP confinement showed enhanced resistance to reversed loadings, the specimens under both static and cyclic loadings exhibits similar stress relaxation performance.
- SEM photo analysis also stated that LCFA-SHCC specimens exhibited superior resistance than HCFA-SHCC specimens under sulfate attack. Moreover, basalt and carbon FRP confined specimens indicated excellent durability performance (indicated a low amount of white deposits) than unconfined specimens. SEM analysis also showed that sulfate penetration to the specimens begun from the outer surface and progressed to the inside of the cylinder specimens and it decreased the bond between PVA fibers and SHCC matrix, deteriorated the interfacial transition zone as reported by the earlier studies.
- Due to the sensitivity of the epoxy resin to alkaline conditions, BFRP and CFRP fabrics are also substantially influenced by the sulfate solution. However, due to the superior high bond between CFRP fabric and the epoxy, CFRP fabrics were less influenced by sulfate attack than BFRP fabrics.
- Statistical analysis also indicated that LCFA-SHCC specimens exhibit superior performance than HCFA-SHCC specimens and the FRP confinement was found to be the much more effective factor on the performance of SHCC specimens. In addition, FRP confinement exhibits a significant effect on the sulfate deteriorated specimens which can be concluded that both FRP fabrics can be used as a rehabilitation material in the sulfate environments.

Conflict of interest

None.

References

[1] J. Qiu, E.-H. Yang, Micromechanics-based investigation of fatigue deterioration of engineered cementitious composite (ECC), Cem. Concr. Res. 95 (2017) 65–74, https://doi.org/10.1016/j.cemconres.2017.02.029.

[2] H. Liu, Q. Zhang, V. Li, H. Su, C. Gu, Durability study on engineered cementitious composites (ECC) under sulfate and chloride environment, Constr. Build. Mater. 133 (2017) 171–181, https://doi.org/10.1016/j.conbuildmat.2016.12.074.

[3] A.W. Herrmann, ASCE 2013 Report Card for America's Infrastructure, IABSE Symp. Rep., Int. Assoc. Brg. Struct 99 (2013) 9–10.

[4] P. Sadeghian, R. Seracino, B. Das, G. Lucier, Influence of geometry and fiber properties on rupture strain of cylindrical FRP jackets under internal ICE pressure, Compos. Struct. 192 (2018) 173–183, https://doi.org/10.1016/j.compstruct.2018.02.077.

[5] M.F. Green, L.A. Bisby, A.Z. Fam, V.K.R. Kodur, FRP confined concrete columns: behaviour under extreme conditions, Cem. Concr. Compos. 28 (2006) 928–937, https://doi.org/10.1016/j.cemconcomp.2006.07.008.

[6] C.-G. Cho, Y.-Y. Kim, L. Feo, D. Hui, Cyclic responses of reinforced concrete composite columns strengthened in the plastic hinge region by HPFRC mortar, Compos. Struct. 94 (2012) 2246–2253, https://doi.org/10.1016/j.compstruct.2012.01.025.

[7] AC125, Acceptance criteria for concrete and reinforced and unreinforced masonry strengthening using fiber-reinforced polymer (FRP) composite systems, ICC Eval. Serv. Whittier, CA. (1997).

[8] ACI Committee 440, ACI 440.2R-02: Guide for the Design and Construction of Externally Bonded FRP Systems for Strengthening Concrete Structures, Farmingt. Hills, Mich Am. Concr. Inst. (2003).

[9] FBI, Externally bonded FRP reinforcement for RC structures, Int. Fed. Struct. Concr. Lausanne, Switz. (2001).

[10] TR 55, Design guidance for stengthening concrete structures using fibre composite materials, Concr. Soc. Camberley, Surrey, Engl. (2004).

[11] H.R. Hamilton, B. Benmokrane, C.W. Dolan, M.M. Sprinkel, Polymer materials to enhance performance of concrete in civil infrastructure, Polym. Rev. 49 (2009) 1–24, https://doi.org/10.1080/15583720802656153.

[12] S. Halliwell, FRPs-the environmental agenda, Adv. Struct. Eng. 13 (2010) 783–791, https://doi.org/10.1260/1369-4332.13.5.783.

[13] A. Nanni, N.M. Bradford, FRP jacketed concrete under uniaxial compression, Constr. Build. Mater. 9 (1995) 115–124, https://doi.org/10.1016/0950-0618(95)00004-Y.

[14] J.M.L. Reis, A.J.M. Ferreira, The effects of atmospheric exposure on the fracture properties of polymer concrete, Build. Environ. 41 (2006) 262–267, https://doi.org/10.1016/j.buildenv.2004.12.017.

[15] J. Marchand, E. Samson, Y. Maltais, J.J. Beaudoin, Theoretical analysis of the effect of weak sodium sulfate solutions on the durability of concrete, Cem. Concr. Compos. 24 (2002) 317–329, https://doi.org/10.1016/S0958-9465(01)00083-X.

[16] A.M. Neville, Properties of Concrete, 4th ed., Longman Group Limited, London, 1995.

[17] C. Wu, V.C. Li, Thermal-mechanical behaviors of CFRP-ECC hybrid under elevated temperatures, Compos. Part B Eng. 110 (2017) 255–266, https://doi.org/10.1016/j.compositesb.2016.11.037.

[18] M.L. Moretti, E. Arvanitopoulos, Overlap length for confinement of carbon and glass FRP-jacketed concrete columns, Compos. Struct. 195 (2018) 14–25, https://doi.org/10.1016/j.compstruct.2018.04.038.

[19] M.V. Seica, J.A. Packer, FRP materials for the rehabilitation of tubular steel structures for underwater applications, Compos. Struct. 80 (2007) 440–450, https://doi.org/10.1016/j.compstruct.2006.05.029.

[20] Reichhold, FRP Material Selection Guide, Triangle Park. NC Reichhold, Inc. (2009).

[21] S. Kumar, N. Sharma, B.C. Ray, Acidic Degradation of FRP Composites, In Proc. the Natl. Conf. Dev. Compos., India, 2007.

[22] M. Sahmaran, M. Li, V.C. Li, Transport properties of engineered cementitious composites under chloride exposure, Mater. J. 104 (2007) 604–611.

[23] M. Sahmaran, M. Lachemi, K.M.A. Hossain, R. Ranade, V.C. Li, Influence of aggregate type and size on ductility and mechanical properties of engineered cementitious composites, Mater. J. 106 (2009) 308–316.

[24] D. Meng, T. Huang, Y.X. Zhang, C.K. Lee, Mechanical behaviour of a polyvinyl alcohol fibre reinforced engineered cementitious composite (PVA-ECC) using local ingredients, Constr. Build. Mater. 141 (2017) 259–270, https://doi.org/10.1016/j.conbuildmat.2017.02.158.

[25] K. Tosun-Felekoğlu, B. Felekoğlu, R. Ranade, B.Y. Lee, V.C. Li, The role of flaw size and fiber distribution on tensile ductility of PVA-ECC, Compos. Part B Eng. 56 (2014) 536–545, https://doi.org/10.1016/j.compositesb.2013.08.089.

[26] E.H. Yang, M. Sahmaran, Y. Yang, V.C. Li, Rheological control in production of engineered cementitious composites, Mater. J. 106 (2009) 357–366.

[27] Baldvin Einarsson, Experimental Research on BFRP Confined Concrete Columns, Master Thesis/Reykjavík Univ. (2011).

[28] ASTM C267 - 01, Standard Test Methods for Chemical Resistance of Mortars, Grouts, and Monolithic Surfacings and Polymer Concretes (2012).

[29] ASTM C39/C39M-12, Standard test method for compressive strength of cylindrical concrete specimens (2012).

[30] S.E. Wallah, B. V. Rangan, Low-Calcium Fly Ash-Based Geopolymer Concrete: Long-Term Properties (2006).

[31] E.K. Attiogbe, S.H. Rizkalla, Response of concrete to sulfuric acid attack, ACI Mater. J. 85 (1988) 481–488.

[32] S.U. Al-Dulaijan, D.E. Macphee, M. Maslehuddin, M.M. Al-Zahrani, M.R. Ali, Performance of plain and blended cements exposed to high sulphate concentrations, Adv. Cem. Res. 19 (2007) 167–175.

[33] S. Thokchom, P. Ghosh, S. Ghosh, Performance of fly ash based geopolymer mortars in sulphate solution, J. Eng. Sci. Technol. Rev. 3 (2010) 36–40.

[34] I. Soroka, in: Portland Cement Paste and Concrete, Macmillan Press, London, 1979, p. 151.

[35] Z. Zhang, Q. Zhang, Self-healing ability of engineered cementitious composites (ECC) under different exposure environments, Constr. Build. Mater. 156 (2017) 142–151, https://doi.org/10.1016/j.conbuildmat.2017.08.166.
[36] Victor C Li, G. Fischer, Reinforced ECC-An evolution from materials to structures, (2002).
[37] N.K. Photiou, L.C. Hollaway, M.K. Chryssanthopoulos, Strengthening of an artificially degraded steel beam utilising a carbon/glass composite system, Constr. Build. Mater. 20 (2006) 11–21, https://doi.org/10.1533/9781845690649.3.274.
[38] M. Demers, K.W. Neale, Confinement of reinforced concrete columns with fibre-reinforced composite sheets-an experimental study, Can. J. Civ. Eng. 26 (1999) 226–241, https://doi.org/10.1139/L07-069.
[39] P. Li, Y.F. Wu, Y. Zhou, F. Xing, Stress-strain model for FRP-confined concrete subject to arbitrary load path, Compos. Part B Eng. 163 (2019) 9–25, https://doi.org/10.1016/j.compositesb.2018.11.002.
[40] H.M. Elsanadedy, Y.A. Al-Salloum, S.H. Alsayed, R.A. Iqbal, Experimental and numerical investigation of size effects in FRP-wrapped concrete columns, Constr. Build. Mater. 29 (2012) 56–72, https://doi.org/10.1016/j.conbuildmat.2011.10.025.
[41] F. Ribeiro, J. Sena-Cruz, F.G. Branco, E. Júlio, Hybrid FRP jacketing for enhanced confinement of circular concrete columns in compression, Constr. Build. Mater. 184 (2018) 681–704, https://doi.org/10.1016/j.conbuildmat.2018.06.229.
[42] K. Lau, L. Zhou, The mechanical behaviour of composite-wrapped concrete cylinders subjected to uniaxial compression load, Compos. Struct. 52 (2001) 189–198, https://doi.org/10.1016/S0263-8223(00)00167-7.
[43] V. Tamuzs, R. Tepfers, C.S. You, T. Rousakis, I. Repelis, V. Skruls, U. Vilks, Behavior of concrete cylinders confined by carbon-composite tapes and prestressed yarns 1 Experimental data, Mech. Compos. Mater. 42 (2006) 13–32.
[44] V. Valdmanis, L. De Lorenzis, T. Rousakis, R. Tepfers, Behaviour and capacity of CFRP-confined concrete cylinders subjected to monotonic and cyclic axial compressive load, Struct. Conc. 8 (2007) 187.
[45] J. Yao, J.G. Teng, J.F. Chen, Experimental study on FRP-to-concrete bonded joints, Compos. Part B Eng. 36 (2005) 99–113, https://doi.org/10.1016/j.compositesb.2004.06.001.
[46] L. Lam, J.G. Teng, C.H. Cheung, Y. Xiao, FRP-confined concrete under axial cyclic compression, Cem. Concr. Compos. 28 (2006) 949–958, https://doi.org/10.1016/j.cemconcomp.2006.07.007.
[47] S.P. Shah, A. Fafitis, R. Arnold, Cyclic loading of spirally reinforced concrete, J. Struct. Eng. 109 (1983) 1695–1710, https://doi.org/10.1061/(ASCE)0733-9445(1983) 109:7(1695).
[48] M.A.M. Ariffin, M.A.R. Bhutta, M.W. Hussin, M. Mohd Tahir, N. Aziah, Sulfuric acid resistance of blended ash geopolymer concrete, Constr. Build. Mater 43 (2013) 80–86, https://doi.org/10.1016/j.conbuildmat.2013.01.018.